Transplantation of Nano-Bioglass/Gelatin Scaffold in a Nonautogenous Setting for Bone Regeneration in a Rabbit Ulna

Article *in* Journal of Materials Science Materials in Medicine · July 2012

DOI: 10.1007/s10856-012-4722-3 · Source: PubMed

6 authors, including:

Forough Hafezi
University of Greenwich
9 PUBLICATIONS **99** CITATIONS
SEE PROFILE

Fatemeh Hosseinnejad
KU Leuven
16 PUBLICATIONS **70** CITATIONS
SEE PROFILE

Abbas Ali Imani Fooladi
256 PUBLICATIONS **2,111** CITATIONS
SEE PROFILE

Afsaneh Amiri
University of Waterloo
31 PUBLICATIONS **228** CITATIONS
SEE PROFILE

J Mater Sci: Mater Med (2012) 23:2783–2792
DOI 10.1007/s10856-012-4722-3

Transplantation of nano-bioglass/gelatin scaffold in a non-autogenous setting for bone regeneration in a rabbit ulna

Forough Hafezi · Fatemeh Hosseinnejad · Abbas Ali Imani Fooladi · Soroush Mohit Mafi · Afsaneh Amiri · Mohammad Reza Nourani

Received: 6 May 2012 / Accepted: 4 July 2012 / Published online: 24 July 2012

Abstract Bioactive glass has been investigated for variety of tissue engineering applications. In this study, fabrication, in vitro and in vivo evaluation of bioactive glass nanocomposite scaffold were investigated. The nanocomposite scaffolds with compositions based on gelatin and bioactive glass nanoparticles were prepared. The apatite formation at the surface of the nanocomposite samples confirmed by Fourier transform infrared spectroscopy, scanning electron microscopy and X-ray powder diffraction analyses. The in vitro characteristics of bioactive glass scaffold as well as the in vivo bone formation capacity of the bioactive glass scaffold in rabbit ulnar model were investigated. The bioactive glass scaffold showed no cytotoxicity effects in vitro. The nanocomposite scaffold made from gelatin and bioactive glass nanoparticles could be deliberated as an extremely bioactive and prospective bone tissue engineering implant. Bioactive glass scaffolds were capable of guiding bone formation in a rabbit ulnar critical-sized-defect model. Radiographic evaluation indicated that successful bridging of the critical-sized defect on the sides both next to and away from the radius took place using bioactive glass scaffolds. X-ray analysis also proposed that bioactive glass scaffolds supported normal bone formation via intramembranous formation

F. Hafezi · F. Hosseinnejad · A. Amiri
Department of Chemistry, Islamic Azad University, Central Tehran Branch, Tehran, Iran

A. A. I. Fooladi
Applied Microbiology Research Center, Baqiyatallah University of Medical Sciences, Tehran, Iran

S. Mohit Mafi
Department of Veterinary, Islamic Azad University, Karaj, Iran

M. R. Nourani (✉)
Tissue Engineering Division, Chemical Injury Research Center, Baqiyatallah University of Medical Sciences, Tehran, Iran
e-mail: r.nourani@yahoo.com

1 Introduction

Our bones give us the freedom to do the things we want to do. They help us to stand up straight, to run, to jump, and to play. That's why it is important for our bones to stay strong and healthy our whole lives long. Many things such as disasters, war injuries, car accidents and health problems including genetic disorders and diseases of the kidneys, lungs, tumors and digestive system can cause osteoporosis and broken bones [1].

Bone tissue has an excellent ability for self-repair of small defects. However, the healing capacity of bone has its limitations. Defects due to trauma or diseases sometimes may not heal by themselves and result in non-union [2].

This situation necessitates the use of bone grafts and bone substitutes to aid in healing. Autografts have long been considered as the gold standard for bone grafts due to their excellent osteoconductivity, osteoinductivity and osteogenicity. Limitations on autografts include donor site morbidity and limited supply. Allografts, being osteoconductive and relatively abundant in supply, have been successfully used in the clinic in bone grafting procedures. Nevertheless, allografts have the potential risk of disease transmission and are inferior in promotion of bone regeneration when compared to autografts due to the required processing, preservation, and sterilization steps. Apart from bone autografts and allografts, a variety of bone graft substitutes exists based on ceramics and polymers [3]. Each has its own advantages, but a variety of concerns still remain.

Among biodegradable and osteoconductive biomaterials such as synthetic porous polymers have proved popular in

current orthopedic surgery. A scaffold plays a critical role in bone tissue engineering by providing structural maintenance of a defect, by contributing a void space for tissue infiltration and vascularization, and by serving as a carrier for therapeutically relevant factors [4, 5].

Bioactive glasses are amorphous, silicate-based materials that bond to bone and imitate new bone growth while dissolving over time, making them candidate materials for tissue engineering [6]. Over a period of 10 years, one of the main goals of bone tissue engineering has been to develop biodegradable materials as bone substitutes for filling large bone defects. In addition, such scaffolds must allow for proper diffusion of oxygen and nutrients to cells embedded into the scaffold as well as proper diffusion of waste from the cells. The final goal is to return full biological and mechanical functionality to a damaged bone tissue. The scaffolds should be biocompatible to the cells and be well integrated into the host tissue without eliciting an immune response, cytotoxicity, or formation of scar tissue [7]. The lack of ideal bone tissue engineering scaffolds necessitates continuous research on new biomaterials and novel scaffold fabrication techniques to facilitate the repair of load-bearing segmental bone defects.

Porous bioglass/gelatin scaffold as a suitable candidate has interconnected pores, which aid in infiltrating osteogenic cells, and is strong enough to maintain implant shape during bone formation [8].

We fabricated nano-bioglass/gelatin scaffold via particulate freeze drying techniques. The purpose of the present study was the evaluation of in vitro and in vivo bone regeneration capacity with nano-bioglass/gelatin scaffolds in a critical-sized rabbit ulnar defect model.

2 Materials and methods

2.1 Materials

Tetraethylorthosilicate (TEOS: $C_8H_{20}O_4Si$), calcium nitrate ($Ca(NO_3)_2{\cdot}4H_2O$), and triethyl phosphate (TEP: $C_6H_{15}O_4P$) and 0.1 M nitric acid (HNO_3), were purchased from Merck Inc. The gelatin used in this research was purchased from Merck (microbiology grade, No. 107040) at 10 % (w/v) concentration. Also, GA ($C_5H_8O_2$) solution of 1 % (w/v) was purchased from Merck Inc.

2.2 Synthesis of bioglass nanopowder

Based on Sol–gel technique, we were able to create Nano Bioglass powder with excellent appropriate structures suitable as artificial matrices for bone tissue engineering.

The Sol–gel-prepared glass materials SiO_2–P_2O_5–CaO (64 % SiO_2, 5 % P_2O_5, and 31 % CaO) (based on mol%), was synthesized and characterized. The solution for the glass was prepared and described as follows: 14.8 g (0.064 mol) of tetraethoxysilane was added into 30 mL of 0.1 M nitric acid, a catalyst for hydrolysis the mixture was allowed to react for 30 min for the acid hydrolysis of TEOS to proceed almost to completion. The following reagents were added in sequence allowing 45 min for each reagent to react completely: 0.85 g (0.005 mol) triethylphosphate, and 7.75 g (0.031 mol) of calcium nitrate tetrahydrate. After the final addition, mixing was continued for 1 h to allow completion of the hydrolysis reaction. The solution was cast in a cylindrical Teflon container and kept sealed for 10 days at room temperature to allow the hydrolysis and a polycondensation reaction to take place until the gel was formed. The gel was kept in a sealed container and heated at 70 °C for an additional 3 days. The water was removed and a small hole was inserted in the lid to allow the leakage of gases while heating the gel to 120 °C for 2 days to remove all the water. Subsequently, the powders were milled by planetary milling (SVD15IG5-1, LG Company) with 400 rpm during 10 h. After grinding and sieving, the dry powder heated 24 h at 700 °C for nitrate elimination. Finally the powder was ground for 10 h for achieving Bioglass (BG) nanopowders [2, 9].

2.3 Scaffold fabrication

The preparation process of these scaffolds is shown in Fig. 1. To fabricate nanocomposite scaffolds, a homogeneous aqueous solution of microbiology-grade gelatin (GEL) (10 % weight per volume, w/v) was prepared and added our synthesized BG nanopowder to obtain a GEL (70)/BG (30) weight composition. After homogenization through stirring, a layer of this composite material was cast into plastic petri dishes (PS), which was subsequently frozen at −20 °C for 3 h to solidify. To produce porous structures, the layers were transferred to a freeze drier (Christ Beta 2-8 LD plus) at −57 °C and 0.05 mbar for 24 h in order to produce 3D porous structure through sublimation to form a gelatin network matrix on the pore walls and the surface of nanocomposite scaffolds. Composite layers were cut at the desired sizes and were laminated by a GEL solution as binding agent (scaffolds with 5 mm diameter × 10 mm length). Next, nanocomposite was soaked in a cross-linking bath of glutaraldehyde (GA) ($C_5H_8O_2$) solution of 1 % (w/v) for 24 h to modify their mechanical properties and render them insoluble in water [10].

2.4 Nano bioglass power characterization

2.4.1 X-ray diffraction (XRD)

X-ray diffraction (XRD) technique (Siemens-Brucker D5000 diffractometer) was used to analyze the crystal structure and

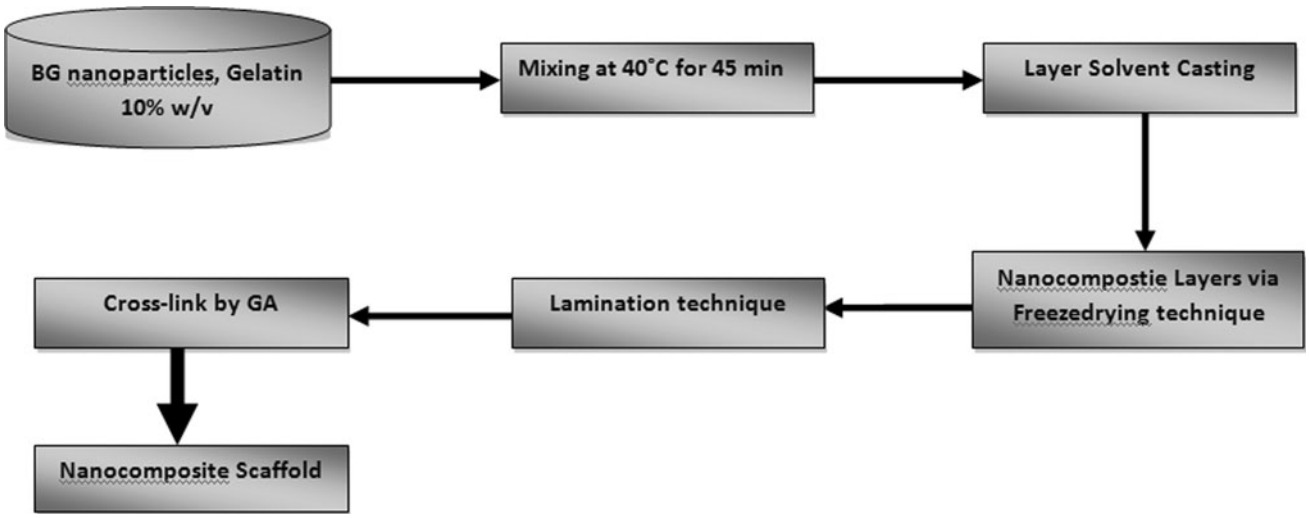

Fig. 1 The manufacturing process of hybrid nanocomposite scaffolds

the phases present in the prepared bioglass. This instrument works with voltage and current settings of 40 kV and 40 mA, respectively, and uses CuKa radiation (1.540600 Å). For qualitative analysis, XRD diagrams were recorded in the interval $10° \leq 2\theta \leq 50°$ at the scan speed of 2° min^{-1}.

2.4.2 Transmission electron microscopy (TEM)

TEM studies were performed with the Philips CM120 operated at 100 kV. The morphology and size of the synthesized BG nanoparticles assessed using TEM by dispersing in ethanol (0.1 g 10 mL^{-1}) and ultrasound for 15 min. Finally, the samples were prepared by placing one drop of nanoparticles dispersion on a carbon-coated grid.

2.4.3 Fourier transforms infrared spectroscopy (FTIR)

The functional groups of nanocomposite scaffolds and the BG nanopowders were examined by FTIR with Bomem MB 100 spectrometer. For IR analysis, in first 1 mg of the powder samples were carefully mixed with 300 mg of KBr (infrared grade) and palletized under vacuum. Then the pellets were analyzed in the range of 400–4,000 cm^{-1} at the scan speed of 120 scan min^{-1} with 4 cm^{-1} resolution.

2.4.4 Scanning electron microscopy (SEM)

The morphology and microstructure of the synthesized BG and nanocomposite samples and measurement of pore size were evaluated using SEM. The nanocomposite samples were coated with a thin layer of Gold (Au) by sputtering (EMITECH K450X, England) and then the morphology of them were observed on a scanning electron microscope (SEM-Philips XL30) that operated at the acceleration voltage of 15 kV.

2.5 In vitro study

2.5.1 Cytotoxicity evaluation

BG scaffolds were sterilized by ethylene oxide at 38 °C for 8 h at 65 % relative humidity. After 24 h aeration in order to remove the residual ethylene oxide, the scaffolds were placed inside a standard 24-well-plate and were washed first with sterile distilled water, after with 0.9 % NaCl sterile solution and finally with culture medium. For cytotoxicity evaluation, Dulbecco's Modified Eagle Medium (DMEM) (GIBCO®) cell culture media containing 10 % (v/v) fetal bovine serum (FBS) and 1 % (v/v) penicillin/streptomycin (P/S) were used. Human airway fibroblast cells with a density of 4×10^5 cell mL^{-1} were added to the samples in PS plates and maintained in incubator (37 °C, CO_2 5 %) for 48 h [11]. Five nanocomposite scaffolds crosslinked with GA 1 % (w/v) were studied for this reason [10]. The samples were fixed in 100 % ethanol for 15 min, and then visualized by light microscopy (Nikon Eclipse 50i) [12].

2.5.2 MTT detection of viable cells

MTT assay is a simple colorimetric assay to measure cell proliferation and viability [13]. Cytotoxicity effects of scaffolds were investigated on Chinese hamster ovary (CHO) cell lines. The cells were plated in 96-well culture plates at 1.7×10^4 cell $well^{-1}$. They were cultured in RPMI-1640 supplemented with 10 % fetal bovine serum (FBS) and 1 % penicillin/streptomycin (P/S) in humidified 5 % CO2 at 37 °C for 24 h. Following the incubation,

mediums were removed and added to the medium interacted with the scaffolds. At the end of 72 h, mediums were removed and 100 µl of fresh medium and 13 µl of MTT solution (5 µg mL^{-1}, diluted with RPMI 1640 without phenol red) were added to the each well. Incubation was allowed for another 4 h in dark at 37 °C. Mediums were removed and 100 µl $well^{-1}$ DMSO (dimethyl sulfoxide) (Sigma-Aldrich, Germany) was added to dissolve formazan crystals. The wells were read at 570 nm on an ELISA plate reader (Tecan Sunrise™) and percentage of viability calculated. The well without scaffold was used as a negative control and cell viability was defined as 100 % for MTT assay control. Each test was repeated three times.

2.6 In vivo implant preparation

The fabricated nano-bioglass/gelatin scaffolds (5 mm diameter × 10 mm length) were sterilized by ethylene oxide at 38 °C for 8 h at 65 % relative humidity. After 24 h aeration in order to remove the residual ethylene oxide, the scaffolds were placed inside a standard 24-well-plate and were washed first with sterile distilled water, next step wash with 0.9 % NaCl sterile solution and finally with culture medium (method previously described) [14].

2.7 Animal surgical procedures

All animal experiments were performed in accordance with the Ethics committee at Baqiyatallah University of medical sciences on the protection of animals used for experimental and other scientific purposes. A total of 15 male New Zealand white rabbits (2.5–3 kg in weight) were used in this study. The experimental groups are listed in Table 1.

Two groups of study were made, 10 randomly selected rabbits were assigned to group (a), five randomly selected rabbits were assigned to group (b) as control group. Rabbits were acclimated for 72 h before surgery after the rabbits were purchased from the Razi Vaccine and Serum Research Institute. One day prior to surgery, 10 mg kg^{-1} enrofloxacin was given to each rabbit intramuscularly. The rabbits were anesthetized using a mixture of ketamine (50 mg kg^{-1}), xylazine (5 mg kg^{-1}), and acepromazine (1 mg kg^{-1}). The right forelimb of the rabbit was shaved, cleaned with betadine and 70 % ethanol. The rabbit was covered with a sterile fenestrated drape to expose the surgical site. A longitudinal incision measuring approximately 20 mm long was made above the ulna. Skin and musculature were then dissected and the mid diaphysis of ulna was exposed. A segment of the ulna measuring 10 mm in length was removed using a reciprocating saw irrigated with 0.9 % sodium chloride saline solution by cutting the ulna 20 mm proximal to the wrist joint and 10 mm proximal to the first cut. Once the segment of ulna was removed and the scaffold was implanted into the defect site (Fig. 2). No fixation device was used. The underlying musculature was then closed using absorbable 3–0 coated VICRYL plus antibacterial (polyglactin 910) suture (Ethicon) and the skin was closed using non-absorbable 3–0 PROLENE blue Monofilament polypropylene suture (Ethicon). Rabbits were kept in recovery cages placed on heating pads and kept under warm light to maintain body temperature. Buprenorphine (0.04 mg kg^{-1}) was administered for 2 days postoperatively every 10 h and then used as needed for pain. The following signs of pain were monitored through frequent observations: grinding of teeth, lack of grooming, sitting haunched up in a corner of the cage, rapid and shallow breathing, reaching less frequently for food and water. Enrofloxacin (10 mg kg^{-1}) was administered for 3 days postoperatively to prevent infection. Animals were allowed full weight-bearing activity and access to food and water. Skin sutures were removed 7–10 days post-surgery.

Table 1 List of the experimental groups, time points and animal assignments

Experimental groups	Radiography	
	Group (a) 5 mm diameter × 10 mm length	Group (b) control
Intact	10	5
After surgery	10	5
2 weeks	10	5
4 weeks	10	5
6 weeks	10	5
8 weeks	10	5
10 weeks	10	5

2.8 Radiographic evaluation

Standardized anteroposterior and lateral radiographs were taken immediately postoperatively and 2, 4, 6, 8, 10 weeks after surgery to monitor the placement of the graft and the bony integration. An ultra-high-definition film (44 kV and 2.2 mA with a constant X-ray to object to film distance of 171 cm) was used.

3 Results

3.1 TEM observations

TEM is a powerful tool for observing the morphology and size of nanoparticles. Figure 3 shows the TEM micrograph of the synthesized BG nanoparticles after heat-treatment at 700 °C. The particles are nearly sphere shaped morphology and the size was in the range of 10–80 nm. This result

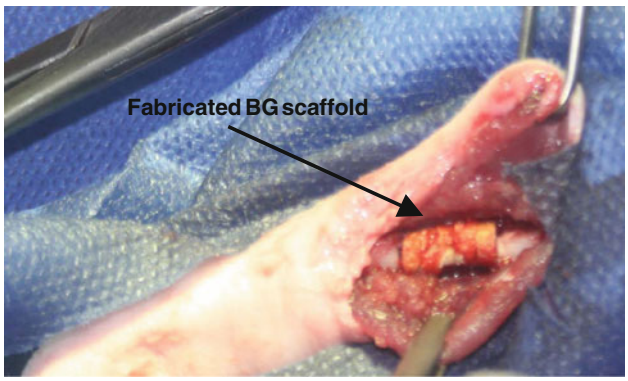

Fig. 2 The surgical procedure showing a 10 mm segment of ulna was removed and a scaffold was implanted into the defect site. The *insert* in shows the porous structure of the s scaffold used in the in vivo study

confirmed the nanoscale size of the synthesized BG nanoparticles.

3.2 XRD analysis

The XRD pattern emphasized the predominant amorphous state of the internal disorder and glassy nature of this material feature of the sample and it is worth mentioning that the BG does not show any crystalline states (Fig. 4).

3.3 FTIR analysis

The FTIR spectra, in the 400–4,000 cm^{-1} spectral range, of BG and scraped material surfaces recorded after synthesis the nanocomposite scaffolds (Figs. 5, 6).

The BG nanoparticles exhibited five infrared bands located at: 609, 800, 930, 1,070 and 1,212 cm^{-1}. Among these bands, those positioned at 800, 930, 1,070 and 1,212 cm^{-1} are related to the silicate network and respectively ascribed to the Si–O symmetric stretching of bridging oxygen atoms between tetrahedrons, Si–O stretching of non-bridging oxygen atoms, Si–O–Si symmetric stretching, and the LO mode of Si–O–Si asymmetric stretching. The band located at 609 cm^{-1} is attributed to the asymmetric vibration of PO4 (Fig. 5). The BG scaffolds also represents the FTIR spectrum of the nanocomposite that exhibited a number of new characteristic spectral bands. The most characteristics of them were protein spectrums such as: N–H bending vibration at 1,260 cm^{-1} for the amide III, N–H bending vibration at 1,560 cm^{-1} for the amide II, C O stretching vibration at 1,670 cm^{-1} for the amide I, C–H bending vibration at 2,952 cm^{-1} for the amide B and band at 3,570 cm^{-1} indicate the presence of O–H groups, while the characteristic spectral bands for BG was present in the Spectrum for nanocomposite too [15, 16] (Fig. 6).

It is worth mentioning that Fig. 6 also shows two peaks which are related to chemical bonds that has been formed

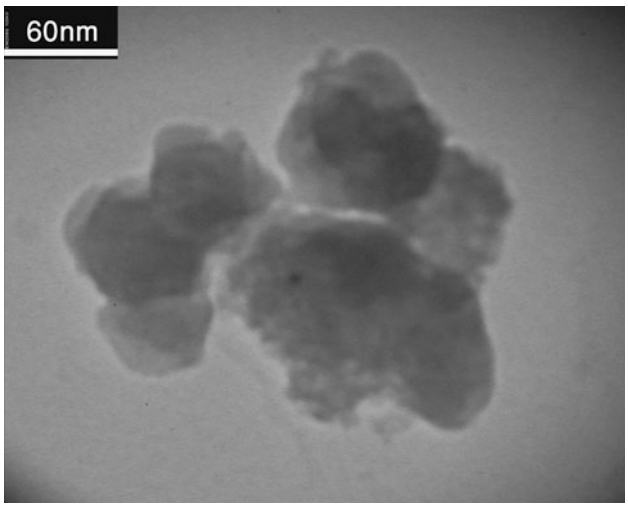

Fig. 3 TEM images of the bioactive nanoparticles

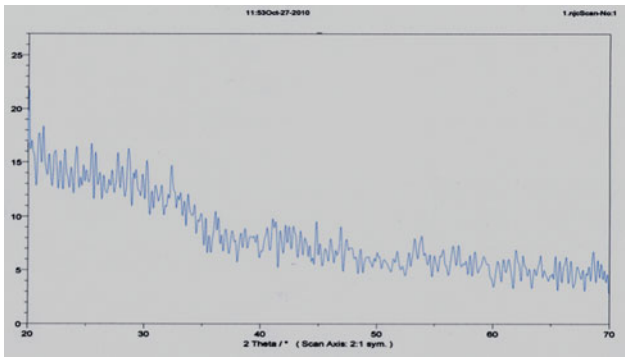

Fig. 4 The XRD pattern of the BG nanoparticles after stabilization at 700 °C

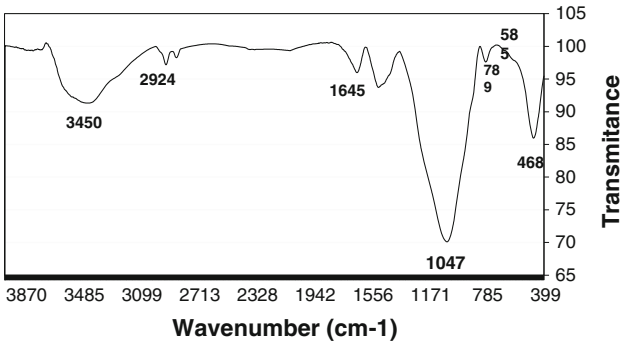

Fig. 5 The FTIR spectra of the synthesized BG nanoparticles

due to the mixture of the BG with gelatin and then cross-linking with GA [15].

3.4 SEM observations

SEM was used to observe the nanocomposite samples morphology. The images captured from surface of porous nanocomposites with SEM (Fig. 7) indicate a network of

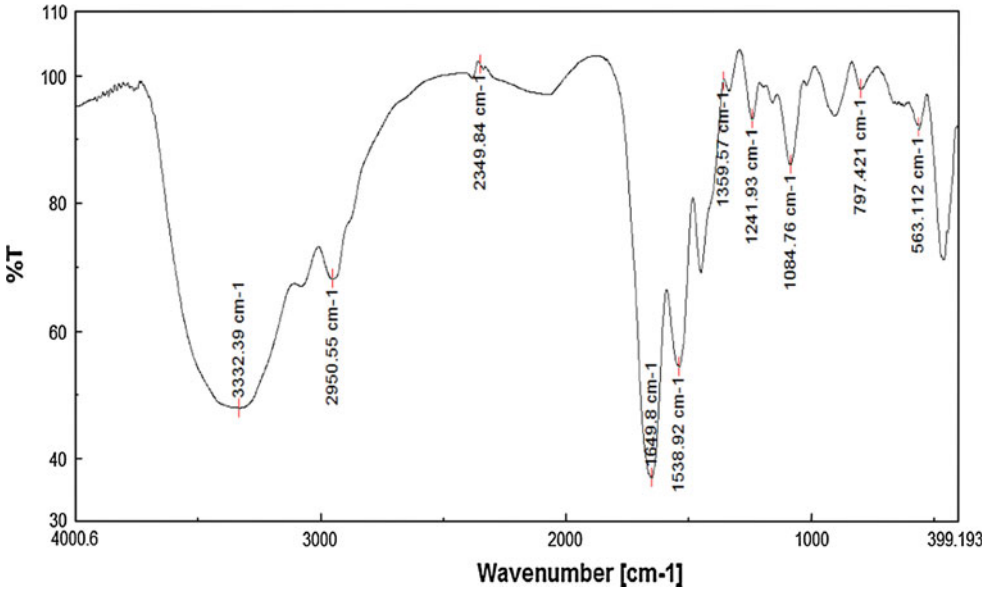

Fig. 6 The FTIR spectra of the prepared nanocomposite scaffold cross-linked by GA

interconnected pores with a fairly uniform spherical shape in top view and deformed elliptical like in the lateral view of layered nanocomposites. The diameter of these pores alters in an almost narrow range and it varies between 300 and 500 μm which is desirable for bone cell growth.

3.5 Sample characterization after in vitro assays

3.5.1 Cytotoxicity evaluation

The biocompatibility of the scaffolds excluding the sample, which was crosslinked with 1 % GA, is distinguished because of the observation of the cellular attachment, spreading and finally developing filopodias. The continuous increase in cell aggregation on the bioactive scaffolds during the 3 days incubation indicated the ability of the scaffolds to support cell growth (Fig. 8).

3.5.2 MTT detection of viable cells

To observe the cytotoxic effects of the produced scaffolds on CHO cell lines in vitro, MTT test was performed. MTT test results were given in Fig. 9.

The results obtained no cytotoxicity effects were significantly observed between results from test and control after 72 h ($Pv > 0.05$).

3.6 Radiographic evaluation

Enlarged radiodensity was ascertained at the defect site from 2 to 10 weeks post-implantation. X-ray graphs during the 10 week period showed that mineralized tissue formation as evidenced by multiplied radiopacity at first took place on the side of the scaffold in the direction of the ulna and at the two distal ends of the synthesized scaffold. A perfect spanning of the defect along the ulna was certified for scaffolds after 2 weeks and thereafter (Fig. 10). Principally, the results indicated that BG scaffold can improve the speed of the bone healing process.

4 Discussion

In brief, the BG nanoparticles were synthesized via Sol–gel method and the BG nanocomposite scaffolds were prepared by layer solvent casting combined with freeze drying and lamination techniques. To investigate the biodegradability of produced scaffolds, fibroblast cells of human lung cultivated under DMEM environment were used. In the next step, the scaffold was installed on ulna of the rabbit. In surgical procedure 10 mm segment of ulna was removed and scaffold was implanted into the defect site, radiograph of the defect immediately after surgery showing the removal of the Segment of ulna. A typical radiograph of the defect site was taken at 2, 4, 6, 8 and 10 weeks post operation.

TEM micrograph showed some agglomeration of the nanopowders due to their high surface area and the results also confirmed that the particles clearly had sizes <100 nm (Fig. 3).

Further studies were reported the same the sizes of the BG particles in their studied and our results confirmed that BG particles have the nano scale sizes [17, 18].

The XRD pattern emphasized the predominant amorphous state of the internal disorder and glassy nature of this material feature of the sample and it is worth mentioning

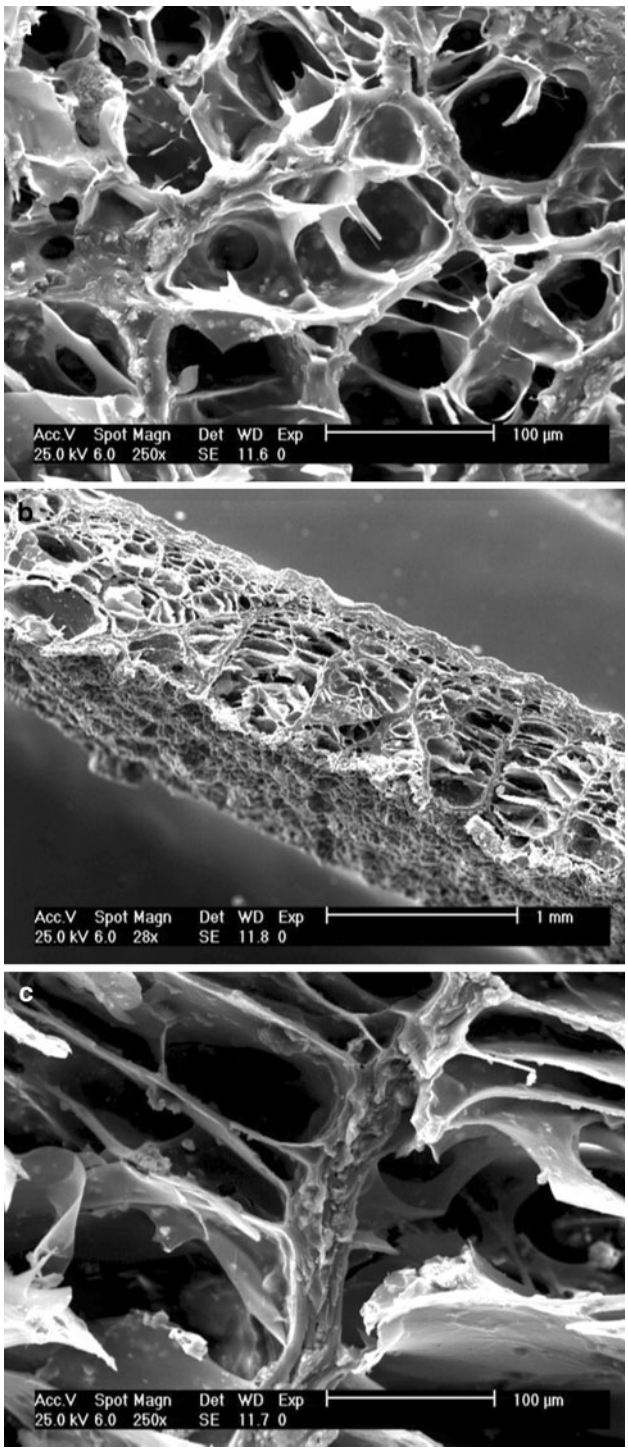

Fig. 7 SEM image of the porous nanocomposite scaffold. **a** High magnification of lateral surface showing fine adhesion between layers, which were glued by GEL solution, **c** High-magnification showing narrow wall thickness between adjacent pores

that the BG does not show any crystalline states. This result confirmed earlier theories of Saravanapavan and FitzGerald [17] concerning to an amorphous phase crystallizing to HCA.

Fourier transform infrared spectroscopy (FTIR) has been proven to be a powerful tool in material characterisation [18]. To study the chemical bonds in engineered nanoBG, the FTIR results obtained from these samples were analyzed. Our data show the FTIR spectra in the 400–4,000 cm^{-1} spectral range revealed that the BG nanoparticles and scraped material surfaces of the nano composite scaffold respectively.

The band located at 585 cm^{-1} is attributed to the asymmetric vibration of PO_4^{3-} [19].

It is noted that the scaffold spectra also shows two peaks which are related to chemical bonds that has been formed due to the mixture of the BG with gelatin and then cross-linking with GA [15].

The first one at about 1,359 cm^{-1} indicates formation of the chemical bond between carboxyl groups from gelatin and Ca^{2+} ions from the BG that has been mentioned in former studies for gelatin and hydroxyapatite [15, 16, 20]. The second bond at 2,349 cm^{-1} appeared after cross-linking of gelatin with GA as mentioned former by Azami et al. [15] (Fig. 6).

By using SEM, the average pore diameter of the nanocomposite samples was observed. SEM Images showed that the foam is comprised of large macropores with diameters in the region of 300–500 µm that are highly interconnected (Fig. 7).

Observed well-interconnected pore network structure and large surface area are necessary for cellular attachment and vascularization [21]. Stock et al. [22] believed that for tissue engineering applications, the most important parameter of the pore network is diameter of the interconnecting pore apertures and the modal interconnected pore diameter should be greater than 100 µm to allow tissue ingrowth and eventually vascularisation. Fu et al. [23] also confirmed that The BG nanocomposite scaffolds which were fabricated through Sol–gel method had the pore size of 100–500 µm.

The cytotoxicity of the BG scaffolds, human airway fibroblast cells were seeded on the scaffolds. Light microscope micrographs showed the biocompatibility of the scaffolds excluding the sample, which was crosslinked with 1 % GA, is distinguished because of the observation of the cellular attachment, spreading and finally developing filopodias. The level of growth observed for cultured cell proves that they could survive and function normally beside scaffolds. Obtained images indicated that the prepared scaffolds had good biocompatibility. Azami et al. [10] confirmed that the most proper GA solution concentration for cross-linking BG nanocomposite aiming at a scaffold for bone tissue engineering is about 1 w/v% solution in distilled water [10] (Fig. 8).

Culturing the scaffold showed that fibroblast cells could grow in the culture media. The general morphology and

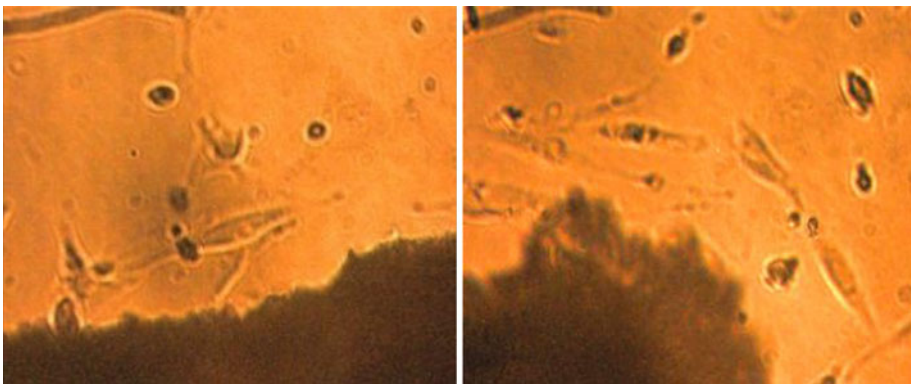

Fig. 8 Human airway fibroblast cells cultured on the produced scaffolds crosslinked with 1 % GA

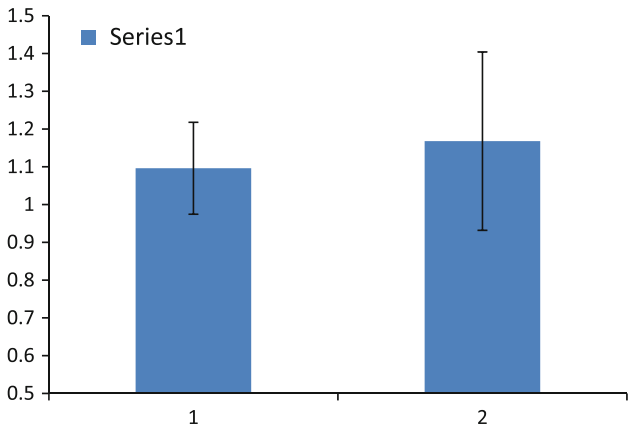

Fig. 9 Cell viability evaluated by MTT assays of BG scaffolds after 72 h. Series 1 and 2 indicate test and negative control samples respectively. No significant differences were observed between the two groups

growth of a cell population and the presence of any microbial contaminants checked regularly under an inverted microscope in phase contrast (Fig. 8) [24].

Our Data obtained from MTT analysis showed no cytotoxic effects on viability and proliferation properties of cells during 72 h. This result clearly suggested that the fabricated scaffolds were nontoxic and posed as good candidates to be used as bone scaffolds. Soňa Jantová and colleagues also applied MTT test to evaluate the biocompatibility and cytotoxicity of bioglass-ceramic composites. Their results illustrated that the bioglass composite showed just a slight cytotoxicity and convenience biocompatibility [25]. Öztürk Güven et al. [26] corroborated that the MTT assay is a good method for determination of cellular viability and cytotoxicity.

The in vivo study showed that a rapid developing process of bone repair was observed in the synthesized scaffold, the primer mineralization started at the bilateral ends of the implant near to the neighbouring bone tissues, progressively reached toward the center of the implant from. The two ends, and there was just a small no-mineral area abided in the center of the implant till 8 weeks post-surgery. This is most likely because the distal ends of the scaffold were in touch with the bone marrow which comprises bone marrow stromal cells, and the part of the scaffold next to the radius was in touch with the periosteum which includes osteoprogenitor cells. Jiang T. and Zhang P. evaluated the in vivo study using the rabbit ulnar critical-sized defect model and porous scaffolds implantation on rabbit's radius respectively. They confirmed that the porous scaffold could guide new bone formation during 12 weeks [27, 28].

5 Conclusion

In this research, nanocomposite scaffolds were produced from a mixture of aqueous gel solution with bioactive synthesized nanostructured glass powder using the Sol–gel method. Then the mentioned mixture was casted in the form of layers and in the next step its water content was sublimed through dry freezing. The stacked layers were latticed in GA solution to enhance layers mechanical strength. Fabrication of the scaffold were carried out through layer casting method and dry freezing process led to creation of a highly porous structure with rather connected unified pore diameters.

To examine biodegradability and biocompatibility of the produced scaffolds, fibroblast cells of human lung cultivated under DMEM environment were used. Performed cellular toxicity test proved no toxicity of the scaffold. It was also revealed biodegradability of the scaffold.

The scaffold was implanted on rabbit's ulna. A typical radiograph of the defect site was taken at 2, 4, 6, 8 and weeks post operation.

Based on the results of this current research, bioactive Sol–gel nanocomposite scaffold made a significant contribution to growth and healing of the bone, as it is hoped to use it as an efficient alternative for the bone in the future.

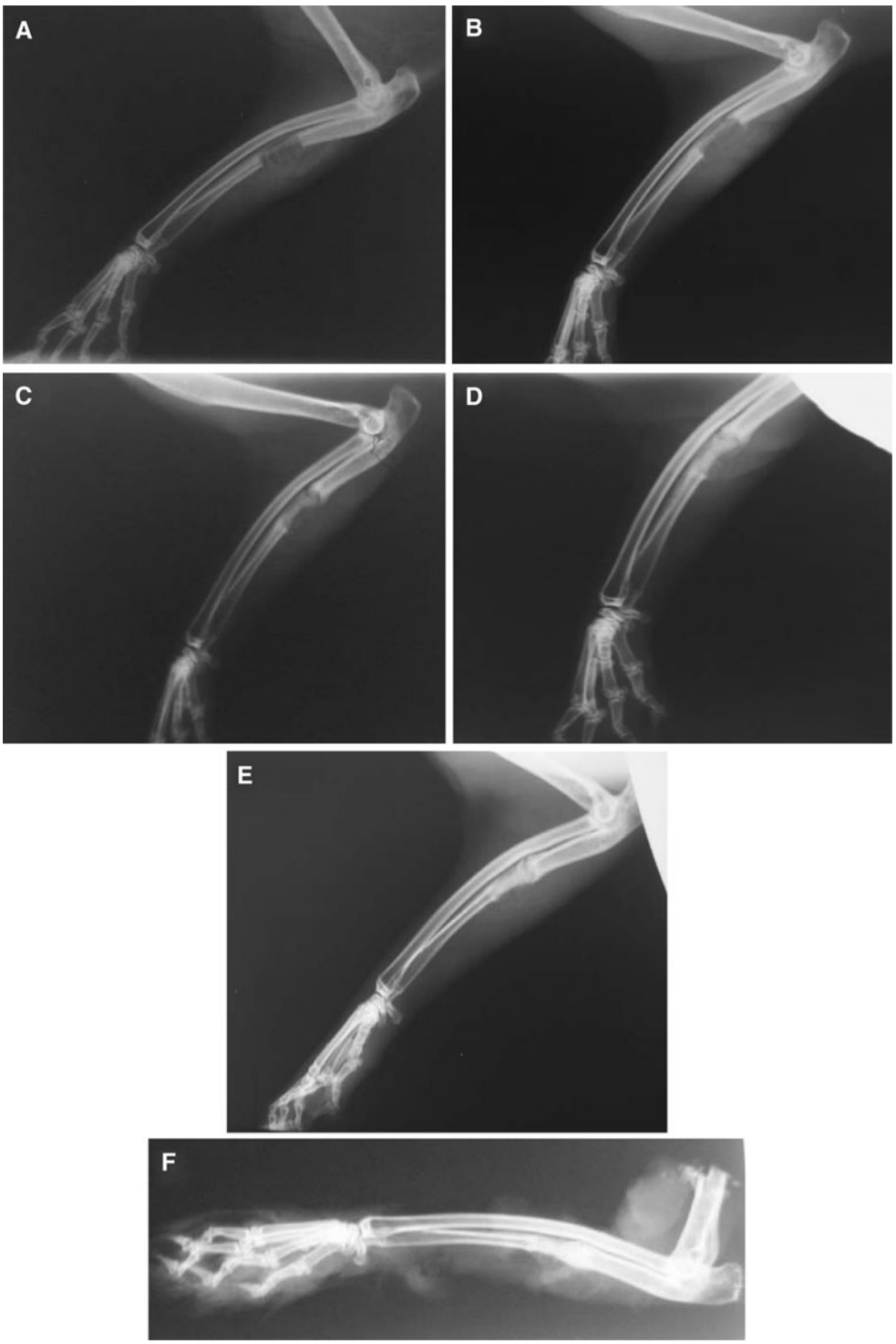

Fig. 10 **a** Radiograph of the defect immediately after surgery showing the removal of the Segment of ulna and the creation of a segmental defect in the ulna, **b–e** typical radiographs of the defect site at 2 weeks (**b**), 4 weeks (**c**), 6 weeks (**d**), 8 weeks (**e**) and 10 weeks (**f**) postoperation in the group (**a**)

Acknowledgments The authors would like to thank many colleagues and collaborators specially Saied Maleknia, and Dr. Mahmoud Azami who have had an enormous role in this research. This work was supported by the grant from the Iranian National Sciences foundation (INSF) and Nano bio technology research center of Baqiyatallah Medical Sciences University.

References

1. Foundation, N.O. National Osteoporosis Foundation; 2011.
2. Schorr A, Campbell W, Schenk M. Communication research and media science in Europe: perspectives for research and academic training in Europe's changing media reality. Berlin: Mouton de Gruyter; 2003.
3. Greenwald AS, et al. Bone-graft substitutes: facts, fictions, and applications. J Bone Joint Surg Am. 2001;83(Suppl 2):98–103.
4. Liu X, Ma PX. Polymeric scaffolds for bone tissue engineering. Ann Biomed Eng. 2004;32(3):477–86.
5. Muschler GF, Nakamoto C, Griffith LG. Engineering principles of clinical cell-based tissue engineering. J Bone Joint Surg Am. 2004;86(7):1541–58.
6. Jones JR, Eilen G, Polak J. Bioactive glass scaffolds for bone regeneration. Elements. 2007;3:393–9.
7. Salgado AJ, Coutinho OP, Reis RL. Bone tissue engineering: state of the art and future. Macromol Biosci. 2004;4(8):743–65.
8. Hoshino M, Egi T, Terai H, Namikawa T, Kato M, Hashimoto Y, Takaoka K. Repair of long intercalated rib defects in dogs using recombinant human bone morphogenetic protein-2 delivered by a synthetic polymer and beta-tricalcium phosphate. J Biomed Mater Res A. 2008;90(2):514–21.
9. Saravanapavan P, Jones JR, Pryce RS, Hench LL. Bioactivity of gel–glass powders in the $CaO–SiO_2$ system: a comparison with ternary ($CaO–P_2P_5–SiO_2$) and quaternary glasses ($SiO_2–CaO–P_2O_5–Na_2O$). J Biomed Mater Res A. 2003;66(1):110–9.
10. Azami M, Rabiee M, Moztarzadeh F. Glutaraldehyde crosslinked gelatin/hydroxyapatite nanocomposite scaffold, engineered via compound techniques. Polym Compos. 2010;31(12):2112–20.
11. Picot J, editor. Human cell culture protocol. New Jersey: Humana Press; 2004.
12. Fassina L, Saino E, Visai L, Avanzini MA, Cusella De Angelis MG, Benazzo F, Van Vlierberghe S, Dubruel P, Magenes G. Use of a gelatin cryogel as biomaterial scaffold in the differentiation process of human bone marrow stromal cells. Conf Proc IEEE Eng Med Biol Soc. 2010;2010:247–50.
13. Mansur HS, Costa HS. Nanostructured poly (vinyl alcohol)/bioactive glass and Poly (vinyl alcohol)/chitosan/bioactive glass hybrid scaffolds for biomedical applications. Chem Eng J. 2008; 137:72–83.
14. Booth AF. Sterilization validation and routine operation handbook: ethylene oxide (sterilization validation and routine operation handbook series). 1st ed. Boca Raton: CRC Press; 1999. p. 121.
15. Azami M, Moztarzadeh F, Tahriri M. Preparation, characterization and mechanical properties of controlled porous gelatin/hydroxyapatite nanocomposite through layer solvent casting combined with freeze-drying and lamination techniques. J Porous Mater. 2010;17:313–20.
16. Tian JT, Tian JM. Preparation of porous hydroxyapatite. J Mater Sci. 2001;36:3061–6.
17. Mortazavi V, Mehdikhani Nahrkhalaji M, Fathi MH, Mousavi SB, Nasr Esfahan B. Antibacterial effects of sol-gel-derived bioactive glass nanoparticle on aerobic bacteria. J Biomedical Materials Research A.2010;94(1):160–8.
18. Mozafari M, Rabiee M, Azami M, Malekni S. Biomimetic formation of apatite on the surface of porous gelatin/bioactive glass nanocomposite scaffolds. J Applied Surface Science. 2010;257(5): 1740–9.
19. Mami M, Lucas-Girot A, Oudadesse H, Dorbez-Sridi R, Mezahi F, Dietrich E. Investigation of the surface reactivity of a sol gel derived glass in the ternary system $SiO_2–CaO–P_2O_5$. Appl Surf Sci. 2008;254:7386–93.
20. Chang MC, Ko CC, Douglas WH. Preparation of hydroxyapatite-gelatin nanocomposite. Biomaterials. 2003;24:2853–62.
21. Jiang L, Li Y, Wang X, Zhang L, Wen J, Gong M. Preparation and properties of nanohydroxyapatite/chitosan/carboxymethyl cellulose composite scaffold. Carbohydr Polym. 2008;74:680–4.
22. Stock SR. X-ray microtomography of materials. Int Mater Rev. 1999;44:141–64.
23. Fu Q, Rahaman MN, Bal BS, Brown RF, Day DE. Mechanical and in vitro performance of 13–93 bioactive glass scaffolds prepared by a polymer foam replication technique. Acta Biomater. 2008;4: 1854–64.
24. Lu HH, El-Amin SF, Scott KD, Laurencin CT. Three-dimensional, bioactive, biodegradable, polymer–bioactive glass composite scaffolds with improved mechanical properties support collagen synthesis and mineralization of human osteoblast-like cells in vitro. J Biomed Mater Res A. 2003;64:465–74.
25. Jantová S, Theiszová M, Matejov P, Bakoš D. Biocompatibility and cytotoxicity of bioglass-ceramic composite with various P_2O_5 content in $Li_2O–SiO_2–CaO–CaF_2–P_2O_5$ system on fibroblast cell lines. Acta Chimica Slovaca 2011;4(1).
26. Öztürk Güven E, Demirbilek M, Sağlam N, Karahaliloğlu Z, Erdal E, Denkbaş EB, Bayram C. Preparation and characterization of polyhydroxybutyrate scaffolds to be used in tissue engineering applications. Hacettepe J Biol Chem 2008;36(4):305–311.
27. Jiang T, Nukavarapu SP, Deng M, Jabbarzadeh E, Kofron MD, Doty SB, Abdel-Fattah WI, Laurencin CT. Chitosan-poly(lactide-co-glycolide) microsphere-based scaffolds for bone tissue engineering: in vitro degradation and in vivo bone regeneration studies. Acta Biomater. 2010;6:3457–70.
28. Zhang P, Hong Z, Yu T, Chen X, Jing X. In vivo mineralization and osteogenesis of nanocomposite scaffold of poly(lactide-co-glycolide) and hydroxyapatite surface-grafted with poly(L-lactide). Biomaterials. 2009;30:58–70.